Neoplasia • Vol. 6, No. 4, July/August 2004, pp. 401–411 401

www.neoplasia.com

Overexpression of Dimethylarginine Dimethylaminohydrolase Enhances Tumor Hypoxia: An Insight into the Relationship of Hypoxia and Angiogenesis *In Vivo*[1]

Vassiliki Kostourou[2], Helen Troy, Joanne F. Murray, Elizabeth R. Cullis, Guy St. J. Whitley, John R. Griffiths and Simon P. Robinson

Department of Basic Medical Sciences, St. George's Hospital Medical School, Cranmer Terrace, London SW17 ORE, UK

Abstract

The oxygenation status of tumors derived from wild-type C6 glioma cells and clone D27 cells overexpressing dimethylarginine dimethylaminohydrolase (DDAH) was assessed *in vivo* using a variety of direct and indirect assays of hypoxia. Clone D27 tumors exhibit a more aggressive and better-vascularized phenotype compared to wild-type C6 gliomas. Immunohistochemical analyses using the 2-nitroimidazole hypoxia marker pimonidazole, fiber optic OxyLite measurements of tumor pO_2, and localized ^{31}P magnetic resonance spectroscopy measurements of tumor bioenergetic status and pH clearly demonstrated that the D27 tumors were more hypoxic compared to C6 wild type. In the tumor extracts, only glucose concentrations were significantly lower in the D27 tumors. Elevated Glut-1 expression, a reliable functional marker for hypoxia-inducible factor-1–mediated metabolic adaptation, was observed in the D27 tumors. Together, the data show that overexpression of DDAH results in C6 gliomas that are more hypoxic compared to wild-type tumors, and point strongly to an inverse relationship of tumor oxygenation and angiogenesis *in vivo*—a concept now being supported by the enhanced understanding of oxygen sensing at the molecular level.

Neoplasia (2004) **6**, 401–411

Keywords: Hypoxia, angiogenesis, DDAH, ADMA, nitric oxide.

Introduction

It is well established that the characteristically chaotic and poorly regulated blood supply of tumors results in hypoxia, and that regions of hypoxia in tumors are resistant to both radiotherapy and chemotherapy [1]. The induction of tumor hypoxia has often been intuitively linked to the inability of the tumor vascular network to provide a nutritive blood supply to the rapidly proliferating tissue [2]. Highly angiogenic tumors should thus be well oxygenated and responsive to both radiotherapy and chemotherapy. However, more recent clinical evidence suggests that sustained tumor hypoxia is associated with cellular changes, resulting in a more malignant phenotype. For example, correlates of high vascular density with necrosis [3] and poor radiotherapeutic [4,5] or chemotherapeutic [6,7] response have been shown, and tumor hypoxia has been associated with poor prognosis and the likelihood of metastasis [8–13]. Taken together, these data suggest that, paradoxically, tumor hypoxia correlates with high vascular density *in vivo* [13]. The most obvious explanation would be that tumor hypoxia induces angiogenesis so effectively that hypoxic tumor tissues are often more angiogenic than oxic tissues. Indeed, hypoxia is a strong stimulus for angiogenesis in numerous pathologic disorders such as wound healing, atherogenesis, and retinopathies [14].

There is currently great interest in the relationship of tumor hypoxia to tumor angiogenesis, and this is being facilitated by the enhanced understanding of the cellular hypoxia response at the molecular level [14,15]. In particular, hypoxia-inducible factor-1 (HIF-1), which is upregulated by low levels of pO_2, activates the transcription of numerous genes whose protein products facilitate adaptation to hypoxia, driving the tumor toward a more malignant phenotype. These include genes encoding glucose transporters, enzymes involved in glycolysis, and angiogenic growth factors such as vascular endothelial growth factor (VEGF) [16,17]. This response is also important in the context of anti–angiogenic strategies designed to treat highly angiogenic tumors.

Nitric oxide (NO) is another important signalling molecule and regulator of angiogenesis [18]. Positive correlations between nitric oxide synthase (NOS) expression and human

Abbreviations: DDAH, dimethylarginine dimethylaminohydrolase; ADMA, asymmetric dimethylarginine; HIF-1, hypoxia-inducible factor-1; Glut-1, glucose transporter-1; VARPRO, variable projection method; 3-APP, 3-aminopropylphosphonate; VEGF, vascular endothelial growth factor

Address all correspondence to: Simon P. Robinson, Department of Basic Medical Sciences, St. George's Hospital Medical School, Cranmer Terrace, London SW17 ORE, UK. E-mail: s.robinson@sghms.ac.uk

[1]This work was supported by the Cancer Research UK (grant C12/A1209), the Royal Society, and St. George's Hospital Medical School. S.P.R. is a recipient of a Royal Society University Research Fellowship and E.R.C. is a recipient of a Royal Society Summer Studentship.

[2]Present address: Vascular Development Laboratory, Cancer Research UK, London Research Institute, 44 Lincoln's Inn Fields, London WC2A 3PX, UK.

Received 6 January 2004; Revised 17 February 2004; Accepted 19 February 2004.

DOI 10.1593/neo.04109

tumor grade have been demonstrated [19–23]. Intracellular factors that regulate NO synthesis may therefore represent important targets in the control of tumor progression. We have recently shown that C6 glioma cells genetically engineered to constitutively overexpress the enzyme dimethylarginine dimethylaminohydrolase (DDAH) result in tumors that grow twice as fast as the wild type [24]. DDAH metabolizes two competitive inhibitors of NO synthesis: asymmetric dimethylarginine (ADMA) and *N*-monomethyl-L-arginine (L-NMMA), indirectly leading to an increase in NO levels both *in vitro* and *in vivo* [25]. ^{1}H magnetic resonance imaging (MRI) studies demonstrated that tumors derived from C6 cells overexpressing DDAH had a greater tumor vascular development and blood volume compared to wild type, and this was confirmed by subsequent histologic analysis [26]. Overexpression of DDAH also increased both the expression and secretion of VEGF [24].

In this study, we have taken advantage of this murine tumor model system expressing a well-defined and characterized phenotypic difference in angiogenesis [24,26], and assessed the oxygenation status of tumors derived from both C6 cells overexpressing DDAH and wild-type cells *in vivo*, using a variety of direct and indirect methods of measuring hypoxia. Specifically, we used: 1) immunohistochemical analysis of the 2-nitroimidazole hypoxia marker pimonidazole [27,28]; 2) the OxyLite/OxyFlo system, which directly measures tumor pO_2 and erythrocyte flow [29–32]; and 3) ^{31}P magnetic resonance spectroscopy (MRS) from which information about the tumor bioenergetic state and pH can be derived and used as a surrogate marker of hypoxia [33,34]. Tumor extracts were also assessed for glucose, lactate, adenosine triphosphate (ATP), and phosphate. In addition, preliminary immunohistochemistry was performed to investigate the expression of the glucose transporter-1 (Glut-1) protein, which is upregulated by hypoxia and is a functional marker of HIF-1 activity [35,36]. Taken together, the data suggest that: 1) constitutive overexpression of DDAH results in the increase of tumor hypoxia compared to C6 wild-type gliomas; and 2) at least in this tumor model system, tumor oxygenation is inversely related to vascular density *in vivo*.

Materials and Methods

Animals and Tumors

Clone 27 (D27) C6 glioma cells, transfected with the full coding region of the rat DDAH I gene, and wild-type C6 cells were used [24]. Cells (2×10^6) were injected into the flanks of female *nu*/*nu* mice under halothane anesthesia. Several cohorts of each tumor type were used and, in each case, the growth rate was monitored to confirm that the D27 tumors grew twice as fast as C6 wild-type tumors, as previously described [24]. For all studies, size-matched D27 and C6 wild-type tumors were used (mean volume ± 1 SEM, 0.79 ± 0.2 cm^3). All experiments were performed in accordance with the UK Home Office Animals (Scientific Procedures) Act 1986.

Fluorescence Microscopy of Hoechst 33342 Uptake and Pimonidazole Immunohistochemistry

Tumor perfusion was assessed by the uptake of the perfusion marker Hoechst 33342 (Sigma, Poole, UK) [26]. Tumor hypoxia was assessed using an immunohistochemical approach following administration of pimonidazole hydrochloride (Hypoxyprobe; Natural Pharmacia International, Research Triangle Park, NC) [27]. Pimonidazole is a 2-nitroimidazole bioreductive chemical probe with an immunorecognizable side chain. Nitroimidazoles undergo a hypoxia-dependent, one-electron reduction catalyzed by cellular reductases, resulting in reactive intermediates that form adducts with cellular components at pO_2 tensions of typically 10 mm Hg or less [27]. Subsequent detection of these adducts by immunohistochemistry can thus give a qualitative assessment of tissue hypoxia.

Mice were administered pimonidazole (60 mg/kg, i.p.). Forty-five minutes later, the mice were administered 15 mg/kg Hoechst 33342 through a lateral tail vein. One minute later, the mice were killed by cervical dislocation and the tumors rapidly excised, frozen, and stored in liquid nitrogen. Serial sections (10 μm) were cut on a cryotome and stored at −80°C until processed. Sections were fixed in ice-cold acetone for 10 minutes and then mounted in phosphate-buffered saline (PBS). Hoechst 33342 fluorescence signals from whole tumor sections were then recorded at 365 nm using a motorized scanning stage (Prior Scientific Instruments Ltd., Cambridge, UK) attached to a BX51 microscope (Olympus Optical Co. Ltd, London, UK), driven by analySIS (Soft Imaging System, Munster, Germany). Digital images from both C6 and D27 tumors were acquired using the same exposure time and composite images then synthesized. Fluorescent particles were detected above a threshold that was constant for all the composite images, and the area of the tumor section with Hoechst 33342 fluorescence determined and expressed as a percentage of the whole tumor section (mean Hoechst-perfused area, mHPA). As the images were acquired and analyzed under identical conditions, any differences in mHPA would result from differences in tumor perfusion.

For pimonidazole staining, the same sections were then incubated first with 2% BSA (wt/vol)/5% goat serum (vol/vol) for 30 minutes, and then with Hypoxyprobe-1 monoclonal antibody (1:10 dilution) (Natural Pharmacia International) for 1 hour at room temperature. Following extensive washing with PBS/0.1% (vol/vol) Tween-20, the sections were then incubated with biotinylated anti–mouse immunoglobulins (1:100 dilution) for 1 hour at room temperature, washed in PBS/0.1% (vol/vol) Tween-20, and incubated with fluorescein streptavidin (1:100 dilution) in the dark for 30 minutes. Regions of pimonidazole adduct formation were detected at 450 to 490 nm using the same fluorescence microscope system, and composite images of whole tumor sections were recorded from the identical stage coordinates, allowing the pimonidazole images to be subsequently overlaid on the Hoechst 33342 images. As for Hoechst 33342, fluorescent particles were detected above a constant threshold, and the area of the tumor section with pimonidazole adduct

fluorescence was determined and expressed as a percentage of the whole tumor section (mean pimonidazole adduct area, mPAA). As the images were acquired and analyzed under identical conditions, any differences in mPAA would result from differences in tumor hypoxia.

OxyLite/OxyFlo Measurements

Mice were anesthesized with a 10-ml/kg intraperitoneal injection of fentanyl citrate (0.315 mg/ml) plus fluanisone (10 mg/ml) ("Hypnorm"; Janssen Pharmaceutical Ltd., High Wycombe, UK), midazolam (5 mg/ml) ("Hypnovel"; Roche, Welwyn Garden City, UK), and water (1:1:2). Tumor pO_2 (mm Hg) was measured using the recently developed fiber optic oxygen-sensing device OxyLite (Oxford Optronix, Oxford, UK). The pO_2 measurements are based on the principle that, following optical excitation of a ruthenium luminophor at the fiber tip, the half-life to return to the ground state is inversely related to the oxygen tension [37]. Precalibrated probes supplied by the manufacturer were used because the response of the sensor to pO_2 is nonlinear. In addition, as the luminescence lifetime is temperature-dependent, pO_2 measurements were corrected automatically for differences in temperature, measured by a thermocouple attached to the OxyLite probe. Coupled to some of the OxyLite probes were laser Doppler OxyFlo probes, which measure erythrocyte flux and hence changes in tumor perfusion at a similar location.

Up to three probes were introduced into each tumor. Each probe was inserted deep into the tumor and then retracted back to sample the tissue pO_2 at five different locations per track. Measurements were made for a minimum of 5 minutes at each location, which was sufficient to allow the sensor to equilibrate to the local oxygen tension prior to obtaining a stable reading for each location. For some locations, the data were rejected as the probe was unable to equilibrate. Data acquisition and averaging were done using Chart version 4 (AD Instruments, Castle Hill, Australia).

^{31}P MRS

For ^{31}P MRS, 1.2 g/kg of the extracellular pH marker 3-aminopropylphosphonate (3-APP) in PBS was injected intraperitoneally about 20 minutes prior to data acquisition [38]. Anesthesized mice were placed in the bore of a 4.7-T horizontal magnet fitted with a 10-G/cm, 12-cm bore high-performance auxiliary gradient insert, interfaced to a Varian UnityInova spectrometer (Varian Inc., Palo Alto, CA), so that the tumors hung into a two-turn ^{31}P surface coil of 10 mm diameter. Body temperature was maintained at *ca.* 37°C with a water-heated pad placed over the mouse. Field homogeneity was optimized by shimming on the water signal for each tumor to a linewidth, typically, of 30 to 50 Hz. The position of the tumor was determined by ^{1}H scout images.

Localized ^{31}P MR spectra were acquired from cuboidal volumes using a modified version of the image-selected *in vivo* spectroscopy (ISIS) technique [39] to minimize signal contamination from underlying tissues. The voxel was selected to exclude nontumor tissue, although in some instances, overlying skin was included. Slice selection employed adiabatic (sin cos) inversion pulses with a gradient strength of 7.5 G/cm. Acquisition employed a hard 90° pulse and a spectral width of 5 kHz with a pulse repetition time of 3 seconds. Because extracellular pH measurements were being made, a double ISIS approach, which produces two spectra (one centered on 3-APP and one centered on α-NTP), was used to minimize the chemical shift artifact introduced due to the wide chemical shift range between 3-APP and α-NTP [40]. Total acquisition time was 52 minutes and 512 transients were averaged for each free induction decay.

Spectral analysis was performed by the variable projection method (VARPRO) time domain nonlinear least squares method, yielding the following peak parameters: areas, frequencies, linewidths, and phases [41]. For each VARPRO analysis, the first four data points were excluded from the fit to eliminate the fast-decaying signals from immobilized phosphates, which cause a baseline hump in the spectra. The data were fitted by assuming contributions from phosphomonoesters (PMEs), inorganic phosphate (P_i), phosphodiesters (PDEs; when visible), phosphocreatine (PCr), and three nucleoside triphosphate (NTP) resonances, and peaks were assumed to be single Lorentzians. The only biochemical and experimental prior knowledge used was that all peaks were assumed to have a phase equal to the overall zero-order phase of the spectrum. In the process of nutritional deprivation as occurs with tumor growth, NTP decreases and P_i increases, so the ratio of "high-energy" to "low-energy" phosphates is used as a measure of the bioenergetic state. The PME resonance primarily consists of the phospholipid metabolites phosphocholine and phosphoethanolamine associated with membrane biosynthesis, and is thus used as an index of proliferation. Relative peak area ratios of the observed phosphates (e.g., βNTP/P_i, $P_i/\Sigma P$, and PME/ΣP) were thus determined from the spectrum centered on α-NTP. ΣP was taken to be the sum of all peaks fitted by VARPRO analysis. Intracellular tumor pH_i was determined by using the VARPRO-derived frequencies for the P_i and α-NTP resonances from the spectrum centered on α-NTP, whereas the extracellular pH was determined using the VARPRO-derived frequency for 3-APP from the spectrum centered on 3-APP.

Tissue Metabolites

Tumors were rapidly excised and freeze-clamped with liquid nitrogen–cooled tongs, followed by extraction with 6% perchloric acid and neutralization. Tissue glucose, lactate, and ATP were measured on the neutralized extracts according to Bergmeyer [42], and phosphate was measured according to ChandraRajan and Klein [43].

Glut-1 Immunohistochemistry

For Glut-1 analysis, C6 (six sections from three separate tumors) and D27 (five sections from three separate tumors) tumor sections were incubated overnight at 4°C in the presence of Glut-1 primary antibody (affinity-pure rabbit anti–rat Glut-1; Alpha Diagnostic International, San Antonio, TX) at a dilution of 1:100. Control sections were incubated with rabbit

IgG (1:100). Secondary antibody treatment (biotinylated anti–rabbit IgG diluted 1:300) and visualization of immunoreactivity with DAB were facilitated by using the Vector ABC kit (Vector Laboratories, Peterborough, UK). The sections were then washed, dehydrated, and mounted. Composite images of whole tumor sections and high-power images were then recorded as described above. A blind semiquantitative analysis was performed using a scale of 0, 1, 2, or 3 to score each section according to the degree of Glut-1 staining observed.

Statistical Analyses

Results are presented in the form mean ± 1 SEM. Significance testing employed the two-tailed Student's *t* test with a 5% confidence level.

Results

Fluorescent composite images of histologic sections obtained from D27 and C6 wild-type tumors stained for the perfusion marker Hoechst 33342 (blue) and reduced adducts of the 2-nitroimidazole hypoxia marker pimonidazole (green) are shown in Figure 1. Both tumor types showed a heterogeneous pattern of distribution of Hoechst 33342 and pimonidazole adduct formation. A greater abundance of Hoechst 33342 staining was associated with the D27 tumors, and the mHPA of the D27 tumors (13.2 ± 2%, $n = 3$, three sections per tumor) was significantly greater than C6 wild-type (7.8 ± 1%, $n = 3$, three sections per tumor, $P < .02$, Student's *t*-test). A greater extent of pimonidazole adduct formation was seen in the D27 tumors (mPAA, 14.1 ± 3%) compared to C6 wild type (mPAA, 11.6 ± 1%), consistent with the greater abundance of reduced cellular intermediates and hence increased tissue hypoxia.

Traces obtained from an OxyLite pO_2 probe (coupled with an OxyFlo Laser Doppler Flowmetry [LDF] probe), inserted into a C6 wild-type glioma and subsequently retracted back through the tumor at five locations as indicated, are shown in Figure 2. The spikes in the LDF trace clearly mark the time of movement of the probe to a new location. There was no trend toward decreasing pO_2 measurements as the probe was retracted through the tumor, suggesting that initial insertion of the probe into the tumor did not induce local hypoxia

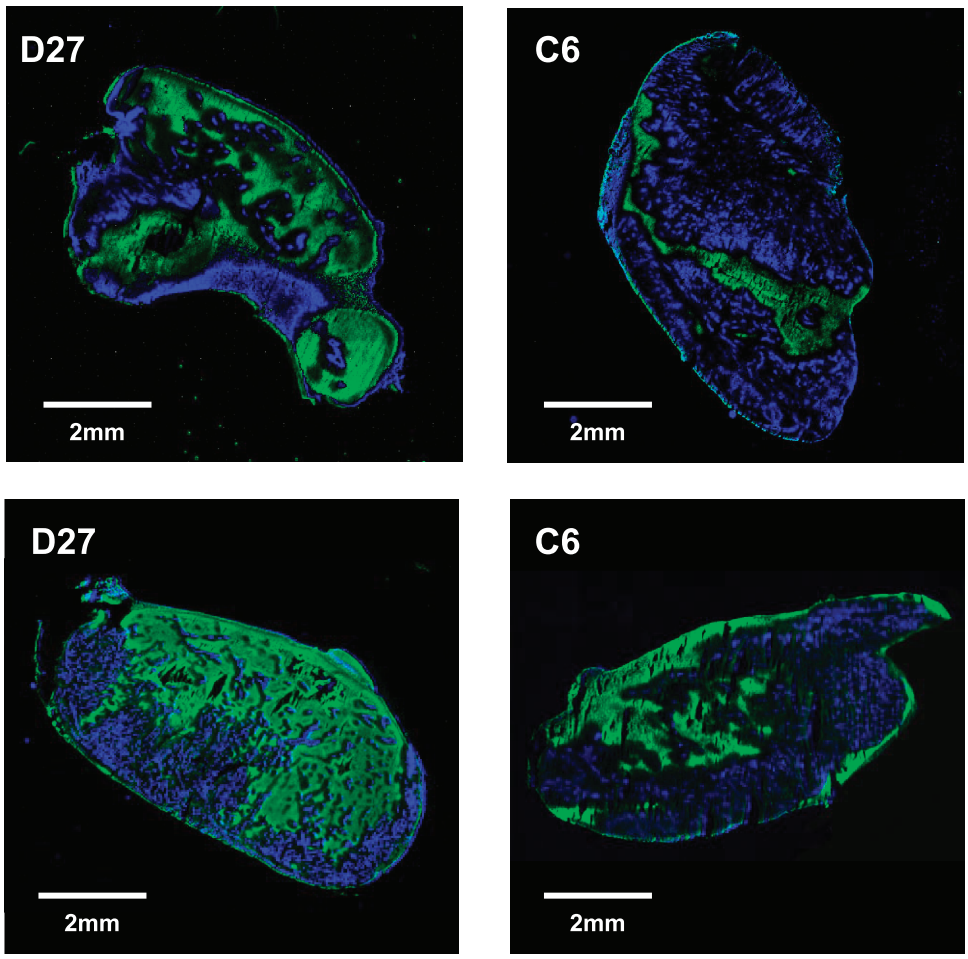

Figure 1. *Composite images of tissue sections obtained from C6 wild type and D27 tumors stained for the perfusion marker Hoechst 33342 and the 2-nitroimidazole hypoxia marker pimonidazole. Tumor blood vessels perfused at the time of injection of Hoechst 33342 appear blue, and regions of pimonidazole adducts fluoresce green by means of biotinylated goat anti–mouse IgG second antibody and fluorescein streptavidin detection. Qualitatively, the D27 tumors exhibited a greater extent of both Hoechst 33342 and pimonidazole staining compared to C6 wild type, consistent with the greater abundance of both perfused blood vessels and increased tissue hypoxia.*

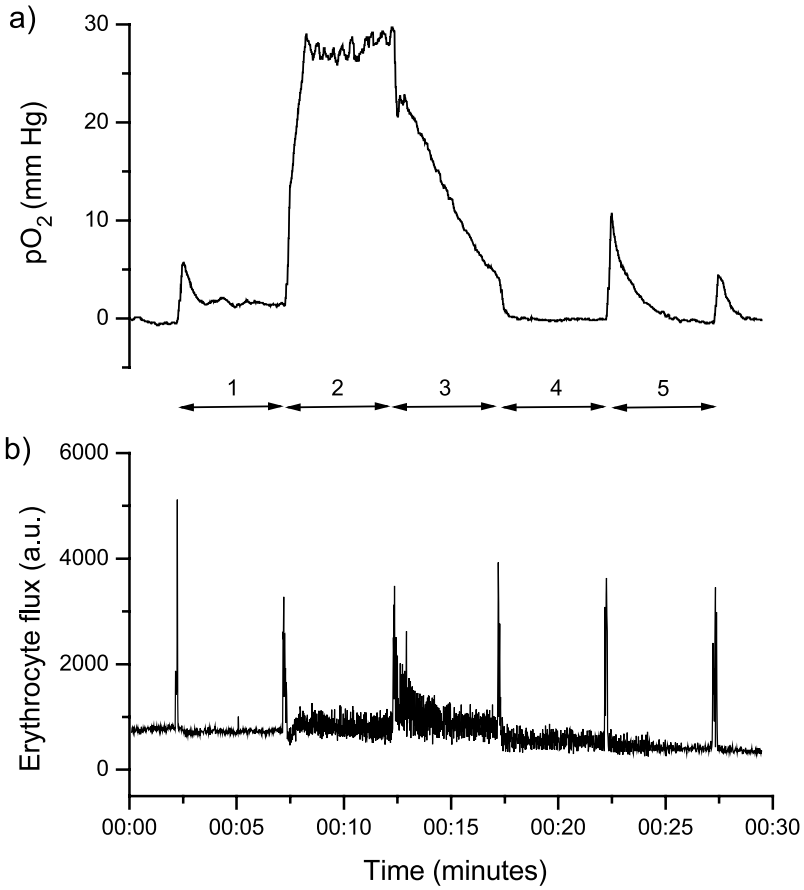

Figure 2. *Traces obtained from (a) one OxyLite pO_2 probe, coupled with (b) an OxyFlo LDF probe, from a C6 wild-type glioma. The probe was inserted into the tumor and then with time retracted back through the tumor to measure the pO_2 at five locations as indicated. The intense spikes in the LDF trace clearly mark the time of movement of the probe.*

through the track. Rather, wide fluctuations were measured in pO_2 at all locations. Note also how relatively high pO_2 was matched with an increase in noise of the LDF trace at locations 2 and 3, suggesting that the probe tips were either within, or proximal to, an area of hemodynamic activity at these locations. The pO_2 measurements were collated as frequency histograms from which the mean and median pO_2, and the percentage of values less than 2.5 mm Hg (considered representative of radiobiologic hypoxia) were determined (Figure 3). The data clearly show that the D27 tumors were significantly more hypoxic than the C6 wild-type gliomas.

Representative localized ^{31}P MR spectra obtained from one D27 and one C6 wild-type tumor are shown in Figure 4. Resonances were typically identified for the 3-APP, PME, P_i, PDE, PCr, γ-NTP, α-NTP, and β-NTP resonances. The spectra shown in Figure 4 were those centered on the α-NTP resonance, hence the poor appearance/phasing of the 3-APP peak. A PDE resonance was clearly resolved in all the C6 wild-type gliomas, but discernible in only one D27 tumor. The ^{31}P MRS results are summarized in Table 1, which show that, compared to C6 wild type, the D27 tumors exhibited a significantly lower bioenergetic state, reflected by the βNTP/P_i and P_i/ΣP ratios, coupled with a more acidic intracellular and extracellular pH. The PME/ΣP ratio, an index of proliferation, was also greater in the D27 tumors compared to C6 wild type but was not statistically significant.

Tissue metabolites were measured enzymatically in extracts of C6 and D27 tumors, and the results are shown in Table 2. Significantly lower concentrations of glucose were measured in the D27 tumors compared to C6 wild type, whereas there was no significant difference between the concentrations of lactate, ATP, or phosphate.

Immunohistochemically stained tumor sections for Glut-1 protein are shown in Figure 5. Glut-1 staining was observed in both tumor types. However, in the sections obtained from D27 tumors, Glut-1 staining was clearly more abundant, whereas in the C6 sections, Glut-1 staining was more diffuse. No Glut-1 staining was apparent in equivalent regions of the control slides (not shown). Accordingly, the semiquantitative analysis of Glut-1 staining revealed a median score of 1 for the C6 sections, whereas a median score of 3 was determined for the sections obtained from D27 tumors.

Discussion

The induction of tumor hypoxia has often been linked to rapidly proliferating tissue outgrowing its nutritive blood supply. Recent clinical data have shown correlates of high

vascular density with both necrosis and poor radiotherapeutic/chemotherapeutic outcome, suggesting the paradox of increasing hypoxia correlating with high vascular density. As an approach to investigate the relationship of angiogenesis and hypoxia, we have taken advantage of a tumor system expressing a well-defined phenotypic difference in angiogenesis through overexpression of DDAH [24,26], and assessed the oxygenation status of these tumors with an array of direct and indirect assays of hypoxia *in vivo*.

The degree of perfusion and hypoxia of wild-type C6 and D27 tumors was assessed by Hoechst 33342 uptake and immunohistochemical detection of reduced adducts of pimonidazole respectively. Tumor uptake of Hoechst 33342 was similar to our previous measurements and again showed a significant increase in the D27 tumors overexpressing DDAH, consistent with increased perfusion [24,26]. The addition of the first electron in the bioreductive activation of pimonidazole is reversibly inhibited by O_2, with half maximal pO_2 of inhibition of about 3 mm Hg and complete inhibition at approximately 10 mm Hg [27]. Using pimonidazole affords a distribution pattern of hypoxic regions throughout a whole tissue section. Pimonidazole adduct formation was evident in both C6 and D27 tumors, similar to that observed in E106 gliomas [30]. However, the D27 tumors clearly showed a greater extent of adduct formation, consistent with their being more hypoxic.

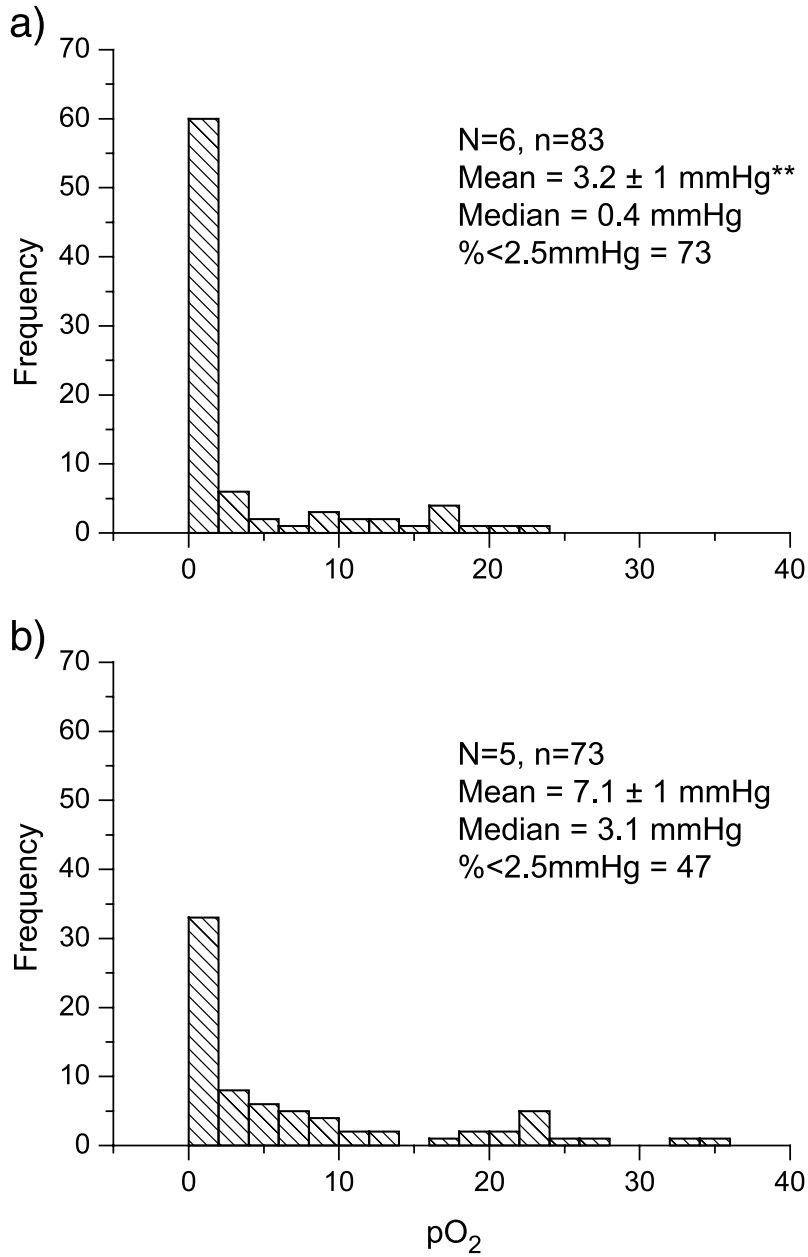

Figure 3. *Frequency histograms of the pO_2 measurements obtained from (a) clone D27 and (b) C6 wild-type tumors. N is the number of tumors studied and n is the total number of individual pO_2 measurements made and used for the data analyses. Results are shown for the mean ± 1 SEM and median pO_2 (in mm Hg), and also the percentage of values less than 2.5 mm Hg, considered indicative of radiobiological hypoxia (**P < .002). The data are consistent with the D27 tumors being significantly more hypoxic.*

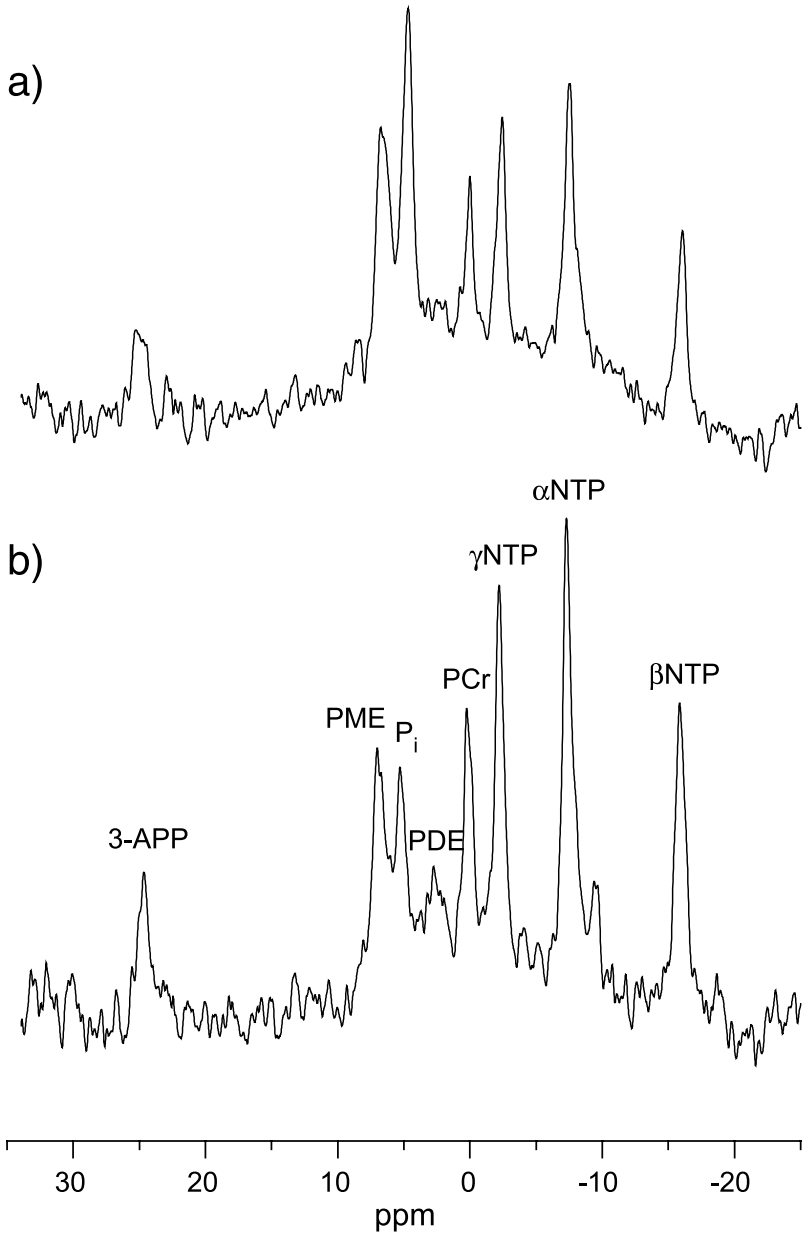

Figure 4. *Representative ISIS-localized ^{31}P MR spectra obtained from (a) one D27 and (b) one C6 tumor. Resonance assignments are: 3-APP, 3-aminopropylphosphonate; PMEs, phosphomonoesters; P_i, inorganic phosphate; PDEs, phosphodiesters; PCr, phosphocreatine; γ-NTP, α-NTP, and β-NTP, nucleoside triphosphate. The spectra shown are those centered on the α-NTP resonance, hence the poor appearance/phasing of the 3-APP peak.*

Tumor pO_2 was measured with fiber optic oxygen-sensing OxyLite probes. One advantage of this approach over other oxygen electrodes is that no oxygen itself is consumed during the measurement process, thus allowing the probe to be left at any one location indefinitely. Furthermore, the signal-to-noise ratio increases with decreasing pO_2, thus making the OxyLite sensor accurate at measuring the low oxygen tensions typically experienced within tumors [37]. The mean pO_2 of the C6 wild-type gliomas was 7.1 mm Hg. This is lower than the mean pO_2 of two other glioblastoma xenografts—the E102 (24 mm Hg) and E106 (18.5 mm Hg)—but greater than the squamous cell xenograft SCCNij3 (4.9 mm Hg) and sarcoma F (2.8 mm Hg), all measured by the OxyLite [30,31]. The mean pO_2 of the D27 tumors, which grow more rapidly and are more vascularized than C6 wild type [24,26], was significantly lower (3.2 mm Hg), consistent with the concept of an inverse relationship between vascular density and pO_2. A similar relationship has also been reported in the clinic. Oxygen measurements of human gliomas with the Eppendorf pO_2 histograph demonstrated significant proportions of hypoxia in glioblastoma [44] and also a small, nonsignificant difference between low-grade and high-grade tumors, with the latter being more hypoxic [45].

Localized ^{31}P MRS, which reports on tumor bioenergetic status and pH, was used to assess the metabolic consequences of hypoxia. Although changes in levels of NTP and P_i cannot strictly be interpreted as changes in tumor

Table 1. Summary of the Localized ^{31}P MRS Data from C6 Wild Type and Clone D27 Tumors.

Tumor	*N*	NTP/P_i	$P_i/\Sigma P$	pH_i	pH_e	PME/ΣP
C6	6	1.9 ± 0.2	0.11 ± 0.01	7.18 ± 0.02	7.10 ± 0.02*	0.14 ± 0.02
D27	6	0.96 ± 0.11†	0.18 ± 0.02†	6.97 ± 0.04†	6.99 ± 0.04‡	0.2 ± 0.01§

N is the number of tumors studied. Results are mean ± 1 SEM. The data are consistent with the D27 tumors having a significantly poorer bioenergetic status, indicated by the significantly lower βNTP/P_i ratio and significantly higher $P_i/\Sigma P$ ratio. The extracellular pH (pH_e) of the C6 gliomas was significantly more acidic than the intracellular pH (pH_i), giving rise to a classic reversed pH gradient. However, in the D27 tumors, there was no significant difference between pH_i and pH_e ($P > .1$). Both pH_i and pH_e were significantly more acidic compared to C6 wild type. The PME/ΣP ratio, an indicator of tissue proliferation, was elevated in the D27 tumors compared to C6 wild type but was not statistically significant.
*$P < .02$.
† $P < .002$.
‡ $P < .03$.
§ $P = .06$.

oxygenation, a more hypoxic tumor would be expected to show depleted high-energy phosphates and increased P_i, coupled with a decline in pH [33]. The bioenergetic status of the D27 gliomas, assessed from the βNTP/P_i and $P_i/\Sigma P$ ratios determined from the ^{31}P MR spectra, was significantly reduced compared to the C6 wild type, again consistent with the more aggressive tumors being more hypoxic.

The measured pH_i and pH_e of the wild-type C6 gliomas were similar to those previously reported [46,47]. The C6 gliomas exhibited the reversed transmembrane pH gradient typical of tumors, with the intracellular pH being maintained at, or greater than, neutrality, whereas the extracellular pH is more acidic [48]. In the D27 tumors, both the intracellular and extracellular pH values were more acidic and no gradient was apparent. The ATP-dependent Na^+/K^+ antiport, which is activated in transformed cells, is one of the key routes used by tumor cells to export protons out into the extracellular space [48]. A recent study showed that this antiport can be nitrosylated by endogenous NO [49]. Elevated NO levels, a consequence of overexpression of DDAH I, may thus impair the function of the ATP-dependent Na^+/K^+ antiport, resulting in a buildup of protons and a lowering of the intracellular pH, eliminating the usual transmembrane pH gradient.

The PME resonance contains contributions primarily from phosphocholine and phosphoethanolamine, phospholipids associated with membrane biosynthesis [34], so the greater PME/ΣP ratio of the D27 tumors compared to wild type reflects the enhanced proliferation rate of these tumors. This, coupled with the observation of a PDE resonance in all the C6 wild-type tumors but not in the more aggressive D27 tumors, is also consistent with a glycerophosphocholine-to-phosphocholine switch, previously shown to be associated with malignant transformation and progression [50].

It has previously been shown that C6 gliomas preferentially use glycolysis for energy production, even in the presence of adequate oxygen concentrations [51]. The determination of tissue glucose, lactate, ATP, and P_i concentrations gives useful information about the steady-state tumor metabolism, which can be related to the oxygenation status of the tumor, but does not inform directly on metabolic rates. Metabolite assays showed a significantly lower concentration of tissue glucose in the D27 gliomas compared to C6 wild type. This is consistent with a higher glucose uptake by the D27 cells and hence a faster metabolic rate. We have previously reported an increased blood volume in the D27 gliomas compared to wild type [26]. A high microvascular blood volume, measured by susceptibility contrast MRI, has been shown to be associated with high glucose uptake, measured by FDG-PET, and tumor angiogenesis in human gliomas [52]. Despite the difference in tissue glucose concentration, there were no significant differences in tissue lactate (the end-product of anaerobic glycolysis), ATP, or P_i concentrations between the two tumor types. Similar lactate concentrations have been measured in C6 gliomas implanted in the rat brain, and lactate has also been shown to be actively turning over, consistent with a predominantly glycolytic metabolism [53,54]. The steady-state tumor extract and ^{31}P MRS measurements, coupled with the enhanced growth rate and blood volume [24,26], are consistent with the enhanced hypoxia in the D27 tumors overexpressing DDAH as a consequence of an increased metabolic rate rather than a limited substrate (glucose) supply. It is likely that kinetic studies would reveal a difference in glycolytic rates, and studies using *in vivo* ^{13}C MRS of D27 and C6 tumors following the infusion of I[^{13}C]-labelled glucose are currently being pursued to address this [55].

Glut-1, which is induced by hypoxia, has been shown to be a reliable functional marker for HIF-1–mediated metabolic adaptation in HIF-1–deficient tumors [35]. Furthermore, clinical evidence suggests that Glut-1 expression is associated with an aggressive phenotype and has prognostic potential [36]. We hypothesized that the measured reduction in glucose concentration in tissue extracts of the D27 tumors may reflect an increase in the expression of glucose transporters through the HIF-1 pathway. Preliminary immunohistochemical studies clearly demonstrated increased focal Glut-1 expression in D27 tumors compared to wild-type

Table 2. Summary of the Tissue Metabolite Concentrations (μmol/g wet wt) Measured Enzymatically from Extracts of C6 Wild Type and Clone D27 Tumors.

Tumor	*N*	Glucose	Lactate	ATP	Phosphate
C6	5	2.54 ± 0.2	7.38 ± 0.8	0.77 ± 0.1	6.59 ± 0.8
D27	5	1.41 ± 0.2*	7.44 ± 0.4	0.75 ± 0.1	5.56 ± 1.1

N is the number of tumors studied. Results are mean ± 1 SEM. Significantly lower concentrations of glucose were measured in the D27 tumors.
*$P < .01$.

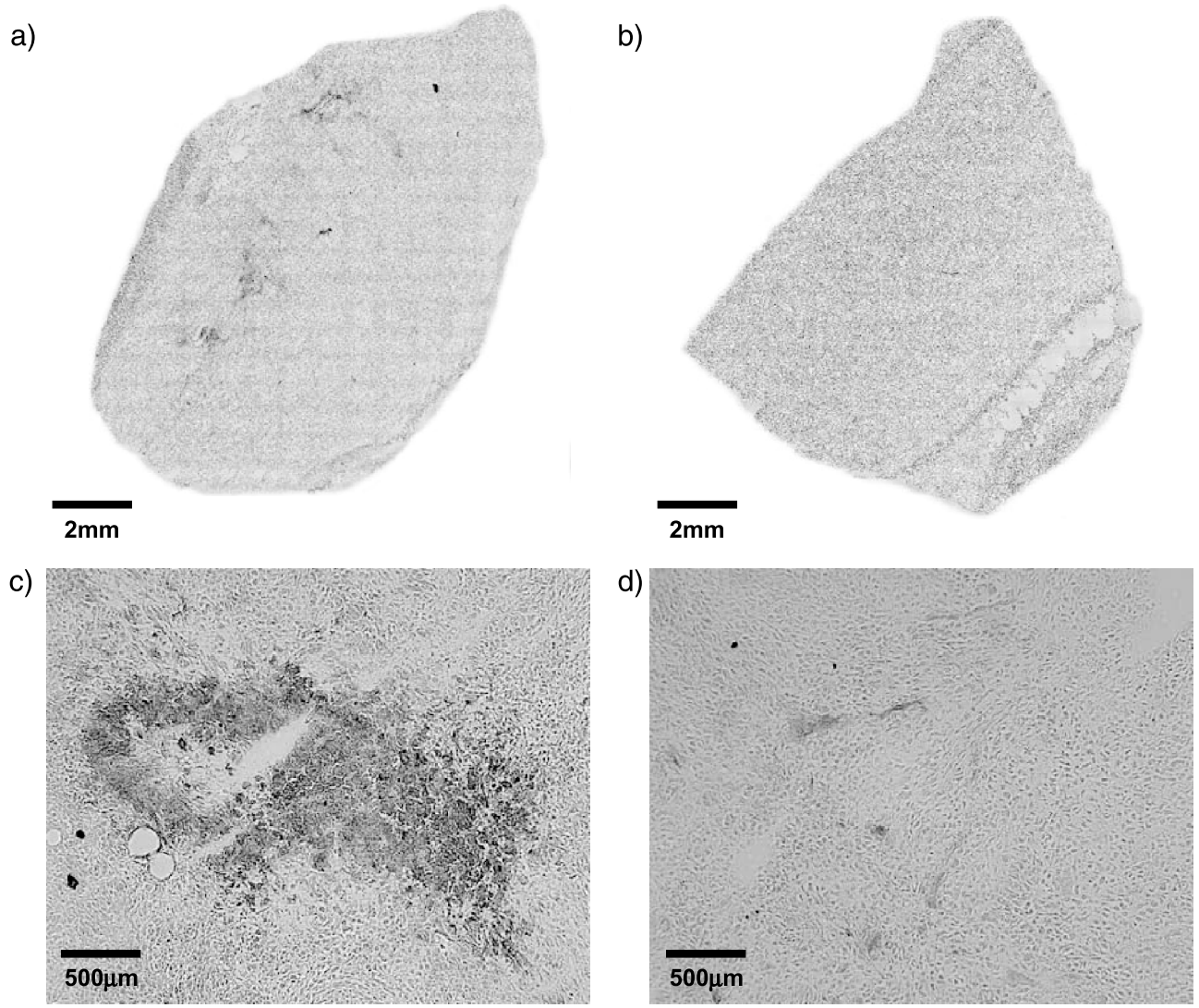

Figure 5. *Composite images of tissue sections obtained from (a) D27 and (b) C6 wild-type tumors immunohistochemically stained for Glut-1 protein and detected by means of immunoperoxidase secondary antibody and DAB chromogen. (c and d) High-power (×100) images of localized regions of intense Glut-1 staining from the same tumor sections in (a) and (b). Glut-1 staining was observed in both tumor types, but was more abundant in sections obtained from D27 tumors.*

C6, supporting a role for the HIF-1 pathway in the adaptation of the D27 tumors to hypoxic stress.

Taken together, the data point toward an inverse relationship of tumor oxygenation and angiogenesis *in vivo* in this tumor system, supporting the hypothesis that increased tumor hypoxia stimulates tumor angiogenesis. We have previously shown that overexpression of DDAH in D27 tumors under normoxic conditions results in an increase in expression and secretion of VEGF compared to wild-type C6 gliomas [24]. This results in the enhancement of tumor blood vessel development, blood volume, and perfused blood vessels in the D27 tumors [24,26], and is consistent with HIF-1–induced VEGF being a survival factor secreted by the tumor cells in response to hypoxic stress.

In summary, we have shown that overexpression of DDAH in C6 gliomas, which we have previously shown to give a more aggressive and better-vascularized phenotype, causes them to be more hypoxic compared to C6 wild-type tumors *in vivo*. The data point strongly to an inverse relationship between tumor oxygenation and angiogenesis *in vivo*, consistent with several recent clinical observations, and is a concept in accordance with the enhanced understanding of oxygen sensing at the molecular level.

Acknowledgements

The authors thank Marion Stubbs for valuable discussions, and Glyn Fisher and his staff for care of the animals.

References

[1] Horsman MR (1998). Measurement of tumor oxygenation. *Int J Radiat Oncol Biol Phys* **42,** 701–704.

[2] Thomlinson RH and Gray LH (1955). The histological structure of some human lung cancers and the possible implications for radiotherapy. *Br J Cancer* **9,** 539–549.

[3] Leek RD, Landers RJ, Harris AL, and Lewis CE (1999). Necrosis correlates with high vascular density and focal macrophage infiltration in invasive carcinoma of the breast. *Br J Cancer* **79,** 991–995.

[4] Cooper RA, Wilks DP, Logue JP, Davidson SE, Hunter RD, Roberts SA, and West CM (1998). High tumor angiogenesis is associated with

poorer survival in carcinoma of the cervix treated with radiotherapy. *Clin Cancer Res* **4,** 2795–2800.

[5] Cooper RA, West CM, Wilks DP, Logue JP, Davidson SE, Roberts SA, and Hunter RD (1999). Tumour vascularity is a significant prognostic factor for cervix carcinoma treated with radiotherapy: independence from tumour radiosensitivity. *Br J Cancer* **81,** 354–358.

[6] Giatromanolaki A, Koukourakis MI, Georgoulias V, Gatter KC, Harris AL, and Fountzilas G (1999). Angiogenesis *vs.* response after combined chemoradiotherapy of squamous cell head and neck cancer. *Int J Cancer* **80,** 810–817.

[7] Koukourakis MI, Giatromanolaki A, Sivridis E, Simopoulos C, Turley H, Talks K, Gatter KC, and Harris AL (2002). Hypoxia-inducible factor (HIF1A and HIF2A), angiogenesis, and chemoradiotherapy outcome of squamous cell head-and-neck cancer. *Int J Radiat Oncol Biol Phys* **53,** 1192–1202.

[8] Brizel DM, Scully SP, Harrelson JM, Layfield LJ, Bean JM, Prosnitz LR, and Dewhirst MW (1996). Tumor oxygenation predicts for the likelihood of distant metastases in human soft tissue sarcoma. *Cancer Res* **56,** 941–943.

[9] Brizel DM, Sibley GS, Prosnitz LR, Scher RL, and Dewhirst MW (1997). Tumor hypoxia adversely affects the prognosis of carcinoma of the head and neck. *Int J Radiat Oncol Biol Phys* **38,** 285–289.

[10] Hockel M, Schlenger K, Aral B, Mitze M, Schaffer U, and Vaupel P (1996). Association between tumor hypoxia and malignant progression in advanced cancer of the uterine cervix. *Cancer Res* **56,** 4509–4515.

[11] Nordsmark M, Overgaard M, and Overgaard J (1996). Pretreatment oxygenation predicts radiation response in advanced squamous cell carcinoma of the head and neck. *Radiother Oncol* **41,** 31–39.

[12] Fyles AW, Milosevic M, Wong R, Kavanagh MC, Pintilie M, Sun A, Chapman W, Levin W, Manchul L, Keane TJ, and Hill RP (1998). Oxygenation predicts radiation response and survival in patients with cervix cancer. *Radiother Oncol* **48,** 149–156.

[13] Koukourakis MI, Giatromanolaki A, Sivridis E, and Fezoulidis I (2000). Cancer vascularization: implications in radiotherapy? *Int J Radiat Oncol Biol Phys* **48,** 545–553.

[14] Carmeliet P and Jain RK (2000). Angiogenesis in cancer and other diseases. *Nature* **407,** 249–257.

[15] Pugh CW and Ratcliffe PJ (2003). Regulation of angiogenesis by hypoxia: role of the HIF system. *Nat Med* **9,** 677–684.

[16] Semenza GL (2000). HIF-1: using two hands to flip the angiogenic switch. *Cancer Metastasis Rev* **19,** 59–65.

[17] Hockel M and Vaupel P (2001). Tumor hypoxia: definitions and current clinical, biologic, and molecular aspects. *J Natl Cancer Inst* **93,** 266–276.

[18] Chinje EC and Stratford IJ (1997). Role of nitric oxide in growth of solid tumours: a balancing act. *Essays Biochem* **32,** 61–72.

[19] Thomsen LL, Lawton FG, Knowles RG, Beesley JE, Riveros-Moreno V, and Moncada S (1994). Nitric oxide synthase activity in human gynecological cancer. *Cancer Res* **54,** 1352–1354.

[20] Thomsen LL, Miles DW, Happerfield L, Bobrow LG, Knowles RG, and Moncada S (1995). Nitric oxide synthase activity in human breast cancer. *Br J Cancer* **72,** 41–44.

[21] Reveneau S, Arnould L, Jolimoy G, Hilpert S, Lejeune P, Saint-Giorgio V, Belichard C, and Jeannin JF (1999). Nitric oxide synthase in human breast cancer is associated with tumor grade, proliferation rate, and expression of progesterone receptors. *Lab Invest* **79,** 1215–1225.

[22] Gallo O, Masini E, Morbidelli L, Franchi A, Fini-Storchi I, Vergari WA, and Ziche M (1998). Role of nitric oxide in angiogenesis and tumor progression in head and neck cancer. *J Natl Cancer Inst* **90,** 587–596.

[23] Cobbs CS, Brenman JE, Aldape KD, Bredt DS, and Israel MA (1995). Expression of nitric oxide synthase in human central nervous system tumors. *Cancer Res* **55,** 727–730.

[24] Kostourou V, Robinson SP, Cartwright JE, and Whitley GS (2002). Dimethylarginine dimethylaminohydrolase I enhances tumour growth and angiogenesis. *Br J Cancer* **87,** 673–680.

[25] MacAllister RJ, Parry H, Kimoto M, Ogawa T, Russell RJ, Hodson H, Whitley GS, and Vallance P (1996). Regulation of nitric oxide synthesis by dimethylarginine dimethylaminohydrolase. *Br J Pharmacol* **119,** 1533–1540.

[26] Kostourou V, Robinson SP, Whitley GS, and Griffiths JR (2003). Effects of overexpression of dimethylarginine dimethylaminohydrolase on tumor angiogenesis assessed by susceptibility magnetic resonance imaging. *Cancer Res* **63,** 4960–4966.

[27] Raleigh JA, Chou SC, Arteel GE, and Horsman MR (1999). Comparisons among pimonidazole binding, oxygen electrode measurements, and radiation response in C3H mouse tumors. *Radiat Res* **151,** 580–589.

[28] Raleigh JA, Chou SC, Bono EL, Thrall DE, and Varia MA (2001). Semiquantitative immunohistochemical analysis for hypoxia in human tumors. *Int J Radiat Oncol Biol Phys* **49,** 569–574.

[29] Braun RD, Lanzen JL, Snyder SA, and Dewhirst MW (2001). Comparison of tumor and normal tissue oxygen tension measurements using OxyLite or microelectrodes in rodents. *Am J Physiol Heart Circ Physiol* **280,** H2533–2544.

[30] Bussink J, Kaanders JH, Strik AM, and van der Kogel AJ (2000). Effects of nicotinamide and carbogen on oxygenation in human tumor xenografts measured with luminescence based fiber-optic probes. *Radiother Oncol* **57,** 21–30.

[31] Collingridge DR, Young WK, Vojnovic B, Wardman P, Lynch EM, Hill SA, and Chaplin DJ (1997). Measurement of tumor oxygenation: a comparison between polarographic needle electrodes and a time-resolved luminescence-based optical sensor. *Radiat Res* **147,** 329–334.

[32] Seddon BM, Honess DJ, Vojnovic B, Tozer GM, and Workman P (2001). Measurement of tumor oxygenation: *in vivo* comparison of a luminescence fiber-optic sensor and a polarographic electrode in the P22 tumor. *Radiat Res* **155,** 837–846.

[33] Tozer GM and Griffiths JR (1992). The contribution made by cell death and oxygenation to ^{31}P MRS observations of tumour energy metabolism. *NMR Biomed* **5,** 279–289.

[34] de Certaines JD, Larsen VA, Podo F, Carpinelli G, Briot O, and Henriksen O (1993). *In vivo* ^{31}P MRS of experimental tumours. *NMR Biomed* **6,** 345–365.

[35] Williams KJ, Telfer BA, Airley RE, Peters HP, Sheridan MR, van der Kogel AJ, Harris AL, and Stratford IJ (2002). A protective role for HIF-1 in response to redox manipulation and glucose deprivation: implications for tumorigenesis. *Oncogene* **21,** 282–290.

[36] Airley R, Loncaster J, Davidson S, Bromley M, Roberts S, Patterson A, Hunter R, Stratford I, and West C (2001). Glucose transporter glut-1 expression correlates with tumor hypoxia and predicts metastasis-free survival in advanced carcinoma of the cervix. *Clin Cancer Res* **7,** 928–934.

[37] Young WK, Vojnovic B, and Wardman P (1996). Measurement of oxygen tension in tumours by time-resolved fluorescence. *Br J Cancer Suppl* **27,** S256–259.

[38] Gillies RJ, Liu Z, and Bhujwalla Z (1994). ^{31}P-MRS measurements of extracellular pH of tumors using 3-aminopropylphosphonate. *Am J Physiol* **267,** C195–203.

[39] Ordidge RJ, Connelly A, and Lohman JAB (1986). Image-selected *in vivo* spectroscopy (ISIS). A new technique for spatially selective NMR spectroscopy. *J Magn Reson* **66,** 283–294.

[40] Ojugo AS, McSheehy PM, McIntyre DJ, McCoy C, Stubbs M, Leach MO, Judson IR, and Griffiths JR (1999). Measurement of the extracellular pH of solid tumours in mice by magnetic resonance spectroscopy: a comparison of exogenous ^{19}F and ^{31}P probes. *NMR Biomed* **12,** 495–504.

[41] van den Boogaart A, Howe FA, Rodrigues LM, Stubbs M, and Griffiths JR (1995). *In vivo* ^{31}P MRS: absolute concentrations, signal-to-noise and prior knowledge. *NMR Biomed* **8,** 87–93.

[42] Bergmeyer H (1974). Methods of Enzymatic Analysis Verlag Chemie, Weinheim.

[43] ChandraRajan J and Klein L (1976). Determination of inorganic phosphorus in the presence of organic phosphorus and high concentrations of proteins. *Anal Biochem* **72,** 407–412.

[44] Rampling R, Cruickshank G, Lewis AD, Fitzsimmons SA, and Workman P (1994). Direct measurement of pO_2 distribution and bioreductive enzymes in human malignant brain tumors. *Int J Radiat Oncol Biol Phys* **29,** 427–431.

[45] Collingridge DR, Piepmeier JM, Rockwell S, and Knisely JP (1999). Polarographic measurements of oxygen tension in human glioma and surrounding peritumoural brain tissue. *Radiother Oncol* **53,** 127–131.

[46] Stegman LD, Ben-Yoseph O, Freyer JP, and Ross BD (1996). *In vivo* ^{31}P MRS evaluation of ganciclovir toxicity in C6 gliomas stably expressing the herpes simplex thymidine kinase gene. *NMR Biomed* **9,** 364–368.

[47] Garcia-Martin ML, Herigault G, Remy C, Farion R, Ballesteros P, Coles JA, Cerdan S, and Ziegler A (2001). Mapping extracellular pH in rat brain gliomas *in vivo* by ^{1}H magnetic resonance spectroscopic imaging: comparison with maps of metabolites. *Cancer Res* **61,** 6524–6531.

[48] Stubbs M, McSheehy PM, Griffiths JR, and Bashford CL (2000). Causes and consequences of tumour acidity and implications for treatment. *Mol Med Today* **6,** 15–19.

[49] Jaffrey SR, Erdjument-Bromage H, Ferris CD, Tempst P, and Snyder SH (2001). Protein *S*-nitrosylation: a physiological signal for neuronal nitric oxide. *Nat Cell Biol* **3,** 193–197.

[50] Aboagye EO and Bhujwalla ZM (1999). Malignant transformation alters

membrane choline phospholipid metabolism of human mammary epithelial cells. *Cancer Res* **59,** 80–84.

[51] Ziegler A, von Kienlin M, Decorps M, and Remy C (2001). High glycolytic activity in rat glioma demonstrated *in vivo* by correlation peak ^{1}H magnetic resonance imaging. *Cancer Res* **61,** 5595–5600.

[52] Aronen HJ, Pardo FS, Kennedy DN, Belliveau JW, Packard SD, Hsu DW, Hochberg FH, Fischman AJ, and Rosen BR (2000). High microvascular blood volume is associated with high glucose uptake and tumor angiogenesis in human gliomas. *Clin Cancer Res* **6,** 2189–2200.

[53] Terpstra M, High WB, Luo Y, de Graaf RA, Merkle H, and Garwood M (1996). Relationships among lactate concentration, blood flow and histopathologic profiles in rat C6 glioma. *NMR Biomed* **9,** 185–194.

[54] Terpstra M, Gruetter R, High WB, Mescher M, DelaBarre L, Merkle H, and Garwood M (1998). Lactate turnover in rat glioma measured by *in vivo* nuclear magnetic resonance spectroscopy. *Cancer Res* **58,** 5083–5088.

[55] Rivenzon-Segal D, Margalit R, and Degani H (2002). Glycolysis as a metabolic marker in orthotopic breast cancer, monitored by *in vivo* ^{13}C MRS. *Am J Physiol Endocrinol Metab* **283,** E623–630.